2011 50th IEEE Conference on Decision and Control and
European Control Conference (CDC-ECC)
Orlando, FL, USA, December 12-15, 2011

Lyapunov based guidance of a mobile sensing agent for state estimation of a gaseous source in a 3D spatial domain

Michael A. Demetriou Nikolaos A. Gatsonis Jeffrey R. Court

***Abstract*— The release of a gaseous substance into the atmosphere can pose a significant risk, whether intentional or accidental. The tracking and localization of the tracer as it moves throughout the domain in real time can provide information on how to minimize subsequent harm. This work investigates the state estimation and real time detection of a continuous source in a 3D environment through a Lyapunov based gradient ascent approach. A set of simulations demonstrate the behavior of the proposed estimator and guidance scheme with different source trajectories. Real time computational results are attained through the use of state reduction and grid adaptation techniques.**

***Index Terms*— Plume dispersion; moving source; mobile sensors; PDEs; grid adaptation; source tracking; state estimation**

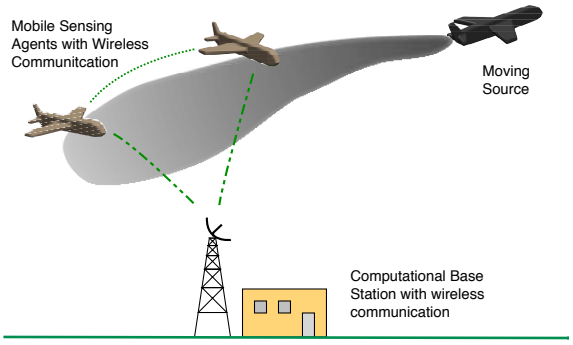

Fig. 1. Proposed Method: moving source detection with a mobile sensing agent.

I. Introduction

The release of a gaseous substance from a land or aerial based source can prose a significant threat. Several approaches have been taken to investigate the detection of a source with mobile sensor networks [1], [2], [3], [4], [5], [6]. Much of the time, these tracking schemes only provide information on the source location. Information on the concentration profile of the material that has already been released can be vary useful in minimizing its impact.

This work builds on previous results [3], [7], [8], [9] by embedding the sensor's dynamic motion into the Lyapunov based guidance scheme. The guidance is determined with a set of desired torques which provide a desired heading and thrust for the mobile sensing agent. The domain is also expanded to a third dimension to account for vertical motion of the source and sensor as well as the vertical motion of the contaminant in the domain. State dependent grid adaptation is used to increase the resolution in the area of interest, while allowing the state estimation to be completed in real time.

Under reasonable stability conditions, the atmospheric advection diffusion equation may be used to model release of an airborne contaminant in the atmosphere. The time varying parameters of the field are assumed known to the model based estimation scheme. This estimation approach has the advantage over other detection schemes through providing an estimate of the entire process state.

Much work has also been done on source localization with extremum seeking (ES) control [10], [11], [12]. Recent work on ES control assumes a single stationary source is to be located. As the ES algorithm runs, the velocity of the agent is tuned with the extremum seeking algorithm to provide an estimate of the gradient of the map. As the results are presented, the agent travels along the highest gradient, and is driven towards the location of the maximum. The current work is different in that it seeks to provide an estimate of the concentration over the entire map instead of just driving the sensor to the location of a maximum within the domain. There are however a couple areas where ES could benefit this work. Instead of using the ES to drive the agent to a maximum concentration, the agent could be driven to areas of higher state estimation error. Also, the tuning element technique from [11] could be applied to the current work to provide the gradient measurement information required by the guidance scheme presented.

The paper presents the control algorithm and estimation scheme as well as the numerical implementation of the approach. Realistic values are used for the atmospheric parameters and mobile agent motion and numerical simulations are provided to demonstrate the performance of the estimation scheme with various realistic source trajectories.

II. Physical modeling

The transport of a contaminant through the troposphere in a 3D domain $\Omega = [0, L_X] \times [0, L_Y] \times [0, L_Z]$ can be modeled with the atmospheric advection diffusion equation [13], [14], [15]. The evolution of the concentration $c(X, Y, Z, t)$ of a

The authors are with Worcester Polytechnic Institute, Dept of Mechanical Engineering, Worcester, MA 01609, USA, {mdemetri,gatsonis,jeff.court}@wpi.edu. The authors gratefully acknowledge financial support from the AFOSR, grant FA9550-09-1-0469.

trace species in the domain can be described by

$$\frac{\partial c}{\partial t} + W_X \frac{\partial c}{\partial X} + W_Y \frac{\partial c}{\partial Y} + W_Z \frac{\partial c}{\partial Z} = \frac{\partial}{\partial X}\left(\kappa_{XX}\frac{\partial c}{\partial X}\right) + \frac{\partial}{\partial Y}\left(\kappa_{YY}\frac{\partial c}{\partial Y}\right) + \frac{\partial}{\partial Z}\left(\kappa_{ZZ}\frac{\partial c}{\partial Z}\right) + S(X,Y,Z,t) \tag{1}$$

where $W(X,Y,Z,t)$ are the wind velocity, $\kappa(X,Y,Z,t)$ are the eddy diffusivities, and $S(X,Y,Z,t)$ is the source term. The initial concentration over the domain is assumed zero $c|_{\partial\Omega} = 0$. The source term can be represented as the product of the release rate $f(t)$ and the spatial distribution $b(X,Y,Z)$. A simple point source is assumed in this work with a time varying centroid at $(X_{c(t)}, Y_{c(t)}, Z_{c(t)})$ and is modeled as a 3D Delta function [16], [17].

$$b(X,Y,Z,t) = \delta(X - X_{c(t)})\delta(Y - Y_{c(t)})\delta(Z - Z_{c(t)}) \tag{2}$$

A. Mobile sensing agent modeling

A mobile agent equipped with sensing capabilities is used to measure the process state at desired locations. The sensor is assumed to measure the concentration $c(X,Y,Z,t)$ at a single point in the domain.

$$y(t) = c(t, X_s, Y_s, Z_s) = \int_0^{L_X}\int_0^{L_Y}\int_0^{L_Z} \delta(X - X_s)\delta(Y - Y_s)\delta(Z - Z_s)c(t,X,Y)\,dX\,dY\,dZ \tag{3}$$

Numerous sensor types are available for measuring atmospheric parameters [18], [19], [20], [21], [22] . Concentration sensors typically provide sensor readings at intervals to account for the transient effects and integration time of the sensor. A specific sensor is not modeled for this work, however a reasonable time between measurements of $2s$ is used. The sensor model also takes into account the fact that any given sensor has a limited range. A maximum and minimum concentration threshold are enforced on the sensing capabilities.

$$c_S(\Theta_s) = \begin{cases} 0 & c(\Theta_s) < c_{min} \\ c(\Theta_s) & c_{min} < c(\Theta_s) < c_{max} \\ c_{max} & c(\Theta_s) > c_{max} \end{cases} \tag{4}$$

where $\Theta_s(t) = (X_s, Y_s, Z_s)$ is the time varying centroid of the sensing agent.

B. Mobile sensing agent motion

In this work, the MSA is assumed to be a fixed wing aerial vehicle that is equiped with a low level autopilot [23], [24], [25], [26]. The kinematic motion of the agent may be expressed in a three dimensional space with $(X(t), Y(t), Z(t))$ representing the position and ϕ, θ, ψ are the attitude angles of the craft. Fixed wing aircrafts have several limitations in their kinematic motion. Finite control forces limit the forward velocity v_{max} as well as the turning velocities $\omega_{\phi,\theta,\psi_{max}}$ of the aerial vehicle. To maintain enough lift, the aerial vehicle must also maintain a minimum forward velocity v_{min} [27], [28], [23].

$$\begin{cases} 0 < v_{min} \le v \le v_{max} \\ -\omega_{\phi,\theta,\psi_{max}} \le \omega_{\phi,\theta,\psi} \le \omega_{\phi,\theta,\psi_{max}} \end{cases} \tag{5}$$

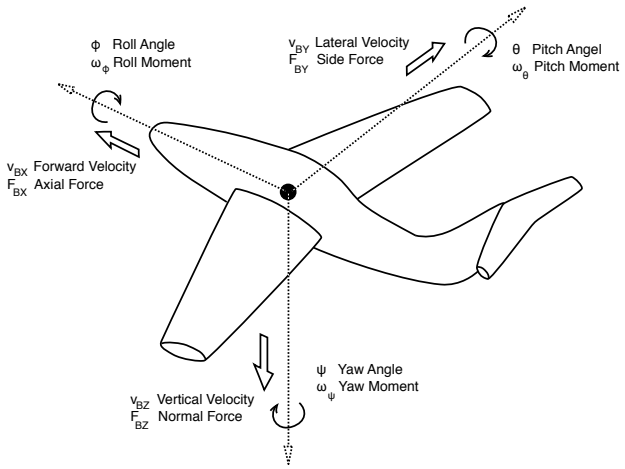

Fig. 2. Sketch of the MSA body coordinate system in 3D.

Although it is not the case for all fixed wing aircrafts, this work assumes the roll ϕ and pitch θ angles of the agent are limited as shown in equation (6). This will prevent the guidance scheme from driving the aircraft into positions that are not common or desirable in flight

$$-\phi_{max} \le \phi \le \phi_{max}, \;\; -\theta_{max} \le \theta \le \theta_{max} \tag{6}$$

In this work, the dynamic motion of an aircraft in 3D can be expressed in body coordinates as [29], [30], [28]

$$\begin{cases} \ddot{X}_B(t) = F_{X_B}(t)/M - \dot{\theta}(t)\dot{Z}_B(t) + \dot{\psi}(t)\dot{Y}_B(t) \\ \ddot{Y}_B(t) = F_{Y_B}(t)/M - \dot{\psi}(t)\dot{X}_B(t) + \dot{\phi}(t)\dot{Z}_B(t) \\ \ddot{Z}_B(t) = F_{Z_B}(t)/M - \dot{\phi}(t)\dot{Y}_B(t) + \dot{\theta}(t)\dot{X}_B(t) \\ \ddot{\phi}(t) = (I_Y - I_Z)\,\dot{\theta}(t)\dot{\psi}(t)/I_X + l(t)/I_X \\ \ddot{\theta}(t) = (I_Z - I_X)\,\dot{\psi}(t)\dot{\phi}(t)/I_Y + m(t)/I_Y \\ \ddot{\psi}(t) = (I_X - I_Y)\,\dot{\phi}(t)\dot{\theta}(t)/I_Z + n(t)/I_Z \end{cases} \tag{7}$$

where $F_{X_B}, F_{Y_B}, F_{Z_B}$ represent the input force in each of the body cartesian directions. On a fixed wing aerial vehicle, the primary force would be the thrust component that is realized in the axial X_B direction. The motion of the aircraft expressed in an inertial, or global, frame can be obtained with a coordinate transformation as

$$v = S^T v_B$$

where v is the velocity vector $(\dot{X}, \dot{Y}, \dot{Z})$ in the inertial frame and v_B is the velocity vector in the body coordinate system. The transformation matrix S^T is expressed as

$$\begin{bmatrix} (C_\psi C_\theta) & (C_\psi S_\theta S_\phi - S_\psi C_\phi) & -C_\psi S_\theta C_\phi - S_\psi S_\phi \\ (S_\psi C_\theta) & (S_\psi S_\theta S_\phi + C_\psi C_\phi) & -S_\psi S_\theta C_\phi + C_\psi S_\phi \\ (-S_\theta) & (C_\theta S_\phi) & (-C_\theta C_\phi) \end{bmatrix}$$

where S and C represent the sine and cosine of the angles respectively [30].

The dynamic equations of motion given in equation (7) have six possible inputs, $F_{X_B}, F_{Y_B}, F_{Z_B}, l, m, n$. On a standard fixed wing aircraft, the forces $F_{Y_B}(t)$ and $F_{Z_B}(t)$ are not induced by the aircraft, but rather wind loading and aircraft weight. For this work, it will be assumed that the low level autopilot applies the correct control forces to adjust them. The remaining four terms are used as control inputs $U = [u_1, u_2, u_3, u_4]$. The thrust component is the longitudinal force $F_{X_B}(t)$ and $l(t), m(t), n(t)$ are the aerodynamic moments created by the control surfaces of the aerial vehicle. The resulting input is then $U = [\dot{v}, \dot{\omega}_\phi, \dot{\omega}_\theta, \dot{\omega}_\psi]$.

$$\begin{cases} \dot{v} = \frac{\tau_{BX}}{M}, \;\; \dot{\omega}_\phi = \frac{l}{I_\phi} \\ \dot{\omega}_\theta = \frac{m}{I_\theta}, \;\; \dot{\omega}_\psi = \frac{n}{I_\psi} \end{cases} \tag{8}$$

III. State estimation with a mobile agent

A. Model based estimator

The estimator developed in [7] is modified to include three dimensional motion and to account for the dynamics of the sensing aerial vehicle. The estimated concentration profile $\widehat{x}(t)$ throughout the entire domain is calculated as

$$\begin{aligned} \dot{\widehat{x}}(t) = &\left(\mathcal{A} - \gamma \mathcal{C}^*(\theta_s(t))\mathcal{C}(\theta_s(t))\right)\widehat{x}(t) \\ &+\gamma \mathcal{C}^*(\theta_s(t)) y(t;\theta_s(t)) \end{aligned} \tag{9}$$

The state error $e(t) = x(t) - \widehat{x}(t)$ is the difference in the actual concentration and the estimated concentration and will be used along with the gradient of the state error for part of the guidance scheme. The error dynamics are then given by

$$\begin{aligned} \dot{e}(t) = &\left(\mathcal{A} - \gamma \mathcal{C}^*(\theta_s(t))\mathcal{C}(\theta_s(t))\right) e(t) \\ &+\mathcal{B}(\theta_c(t)) f(t), \\ e(0) = &\, e_0 \in \mathcal{X}. \end{aligned} \tag{10}$$

B. Mobile sensing agent dynamic guidance

The Lyapunov function used in [7] provides a gradient ascent policy that directs the sensing agent in the direction of the maximum state error in the domain by providing a set of desired velocities. The guidance signal is calculated based on the state error $e(t, X, Y)$ as well as the gradient of the state error $(e_X(t, X, Y), e_Y(t, X, Y))$, at the spatial location of the sensor $\Theta_s(t) = (X_s(t), Y_s(t))$. In this work, that guidance policy is expanded to include a third dimension as well as the kinetic and potential energy of the mobile sensing vehicle and will guide the sensor with input forces.

The Lyapunov equation is modified to include the energy of the system.

$$V = -\left\langle x(t), A_{cl}(X(t), Y(t), Z(t)) x(t) \right\rangle + PE + KE$$

Considering the motion of the MSA in 3D, the energy of the system is added to the Lyapunov function as

$$\begin{aligned} V = &-\left\langle x, A_{cl}(X, Y, Z) x \right\rangle + \tfrac{1}{2} M \dot{X}^2 + \tfrac{1}{2} M \dot{Y}^2 \\ &+\tfrac{1}{2} M \dot{Z}^2 + \tfrac{1}{2} I_\phi \dot{\phi}^2 + \tfrac{1}{2} I_\theta \dot{\theta}^2 + \tfrac{1}{2} I_\psi \dot{\psi}^2 + MgZ \end{aligned} \tag{11}$$

where ϵ is the state error, $\epsilon_X, \epsilon_Y, \epsilon_Z$ are the gradient of the state error, and g is the gravitational acceleration.

$$\begin{aligned} \dot{V} = &-2\left|A_{cl}(X, Y, Z) x\right| - \epsilon\epsilon_X \dot{X} - \epsilon\epsilon_Y \dot{Y} - \epsilon\epsilon_Z \dot{Z} \\ &+M[\dot{X}\ddot{X} + \dot{Y}\ddot{Y} + \dot{Z}\ddot{Z}] + I_\phi \dot{\phi}\ddot{\phi} + I_\theta \dot{\theta}\ddot{\theta} + I_\psi \dot{\psi}\ddot{\psi} + Mg\dot{Z} \end{aligned} \tag{12}$$

The three terms dealing with the angle may be neglected since the orientation of the MSA will not change the sensor readings, just the spatial location of the sensor's centroid. Making the appropriate substitution for the dynamics with equation (7) and focusing on the part of the Lyapunov derivative equation to be made negative definite yields

$$\begin{aligned} &-\epsilon\epsilon_X \dot{X} + M\dot{X}\left[\tfrac{\tau_X}{M} - \dot{\theta} v \sin(\theta) + \dot{\psi} v \cos(\theta)\sin(\psi)\right] \\ &-\epsilon\epsilon_Y \dot{Y} + M\dot{Y}\left[\tfrac{\tau_Y}{M} - \dot{\psi} v \cos(\theta)\cos(\psi) + \dot{\phi} v \sin(\theta)\right] \\ &-\epsilon\epsilon_Z \dot{Z} + M\dot{Z}\left[\tfrac{\tau_Z}{M} - \dot{\phi} v \cos(\theta)\sin(\psi) + \right. \\ &\qquad \left. \dot{\theta} v \cos(\theta)\cos(\psi) + g\right] \end{aligned} \tag{13}$$

where $\tau_X(t), \tau_Y(t), \tau_Z(t)$ are the components of the thrust vector in each Cartesian direction. The guidance scheme is then chosen to be

$$\begin{cases} \tau_X = k_1\epsilon\epsilon_X + k_3 M\left[\dot{\theta} v \sin(\theta) - \dot{\psi} v \cos(\theta)\sin(\psi)\right] \\ \tau_Y = k_1\epsilon\epsilon_Y + k_3 M\left[\dot{\psi} v \cos(\theta)\cos(\psi) - \dot{\phi} v \sin(\theta)\right] \\ \tau_Z = k_2\epsilon\epsilon_Z + k_3 M\left[\dot{\phi} v \cos(\theta)\sin(\psi)\right. \\ \qquad \left. -\dot{\theta} v \cos(\theta)\sin(\psi) - g\right] \end{cases} \tag{14}$$

where $k_1, k_2, k_3 > 0$ are user defined constant guidance gains. Since the state error, error gradient, and velocity of the sensor are a function of time, the contribution of each portion of the guidance scheme will change over time. For this reason, the constant value of k_3 is chosen so that the dynamics portion of the controller is of the same order of magnitude as the state error portion.

The Lyapunov based guidance scheme developed provides a set of desired Cartesian force components $\tau_X^d, \tau_Y^d, \tau_Z^d$. Due to holonomic constraints, the MSA is unable to implement them directly. Instead, they are implemented as a desired thrust component τ_l^d and set of attitude angles ϕ^d, θ^d, ψ^d. The thrust is the magnitude of the desired component forces.

$$\tau_l^d = \sqrt{(\tau_X^d)^2 + (\tau_Y^d)^2 + (\tau_Z^d)^2} \tag{15}$$

The desired yaw and pitch angles come from the angle created by the desired cartesian velocities as

$$\theta^d = \tan^{-1}\left(\frac{\tau_Z^d}{\sqrt{\left(\tau_X^d\right)^2 + \left(\tau_Y^d\right)^2}}\right), \quad \psi^d = \tan^{-1}\left(\frac{\tau_Y^d}{\tau_X^d}\right) \tag{16}$$

The sensor measurements are not affected by the roll angle, so the desired and commanded roll angle will be chosen to be zero. Since the SAV is able to have any yaw

angle, $\psi^c = \psi^d$. The commanded pitch angle is chosen as the saturated value of the desired pitch angle, $-\theta_{max} \leq \theta \leq \theta_{max}$. The desired input to control the MSA can then be built following Equation (8). The first desired input is the thrust term $u_1^d = \tau_l^d$ from equation (15). The three angular torque inputs are chosen to drive the MSA attitude to the desired attitude from equation (16) as quickly as possible. The desired yaw force is calculated as

$$\tau_\psi^d = \left(\psi^c - \psi^a - \omega_\psi \Delta t\right) \frac{I_Z}{\Delta t^2} \tag{17}$$

The desired roll and pitch input torques are calculated in the same manner. The desired inputs U^d are then adjusted to account for the physical limitations of the MSA with a saturation function. The commanded control signals U^c are

$$-U_{max} \leq U^c \leq U_{max} \tag{18}$$

where the maximum values are due to the physical limitations of the MSA.

IV. Numerical Implementation and State Dependent Grid Adaptation

A. Plant simulation

To run the estimator, the forward problem is simulated to generate sensor data. The domain Ω is taken to be a rectangular prism with one surface parallel to the ground. All boundaries are held constant at a zero concentration. The atmospheric advection diffusion equation is solved with a structured finite volume approach. The conservative form of the advection diffusion equation is rewritten in the flux form and integrated over the control volumes [31], [32], [33], [34]. Following the approach by Gatsonis et al. [34], a four stage Runge Kutta scheme is used to explicitly solve equation (19).

Due to the fact that the forward problem is replacing atmospheric measurement data, a relatively high number of cells are used. This ensures a smooth solution profile that provides sensor readings. The domain is discretized with a uniform grid. At each numerical time step, the entire concentration profile is saved so "sensor readings" can be taken by the estimation scheme.

B. Finite dimensional approximation of estimator

The infinite dimensional state estimator given in equation (9) is approximated as a finite dimensional system as

$$\begin{aligned}\dot{\widehat{x}}^n(t) = &\left(A - \gamma C^T(\Theta_s(t))C(\Theta_s(t))\right)\widehat{x}^n(t) \\ &+\gamma C^T(\Theta_s(t))y(t;\Theta_s(t))\end{aligned} \tag{20}$$

where $\widehat{x}^n(t)$ is the finite dimensional representation of the estimated state and A, C are the finite dimensional representation of the infinite dimensional operators $\mathcal{A}, \mathcal{C}$. In order to estimate the state, the estimation scheme assumes knowledge of the domain parameters such as the boundary conditions, wind profile (W_X, W_Y, W_Z), and eddy diffusivities $(\kappa_X, \kappa_Y, \kappa_Z)$ in the domain (L_X, L_Y, L_Z) of interest.

The state estimator uses significantly fewer computational nodes than the forward problem. This allows the estimator computations to be carried out much faster than the forward problem, since real time calculations are important. The reduced dimension also avoids the "inverse crime" [35] problem that can be encountered in inverse problems, which arise when the simulated forward and inverse problems are of the same dimension.

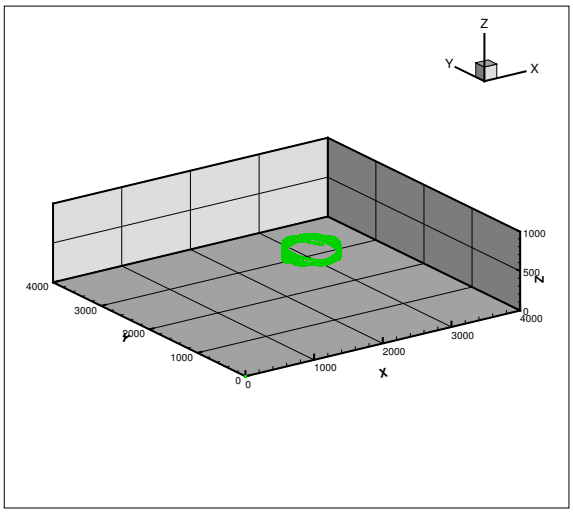

Fig. 3. Typical sensor patrol path

C. MSA patrolling behavior

Although this state estimation and source localization approach can apply to numerous scenarios, this work assumes a scenario where a MSA is tasked with patrolling a fixed area until a non-zero sensor reading is registered. Numerous patrol paths and approaches are possible. However, to minimize the number of agents required to patrol a given region, each agent should patrol as much area as possible. For an agent to patrol the entire domain, a lot of time would be required. Instead, the agent uses knowledge of the domain and patrols a smaller, downwind region of the domain in a circular path with increasing and decreasing altitude, as shown in Figure 3. This search strategy will increase the chance of detecting an intruder in the domain, but is not assumed optimal. Upon detection of an elevated concentration measurement, the agent ceases patrolling and follows the guidance scheme outlined in equation (14).

D. Sensor measurements and guidance from numerical model

The estimation scheme assumes state and gradient measurement data is available at the sensor location. From the simulation of the forward problem, sensor data is available in the stored data file. With a point sensor assumption, the measured concentration is simply the concentration in the finite volume at that location.

$$c(X, Y, Z) = c_{i,j,z}$$

$$\frac{\partial c}{\partial t} + W_X \frac{\partial c}{\partial X} + W_Y \frac{\partial c}{\partial Y} + W_Z \frac{\partial c}{\partial Z} = \kappa_{XX} \frac{\partial^2 c}{\partial X^2} + \kappa_{YY} \frac{\partial^2 c}{\partial Y^2} + \kappa_{ZZ} \frac{\partial^2 c}{\partial Z^2} + bf$$
$$\iiint_V \frac{\partial c}{\partial t} dV + \iiint_V \cdot \nabla c dV = \iiint_V \nabla[\kappa \nabla c] dV + \iiint_V s dV \tag{19}$$
$$\iiint_V \frac{\partial c}{\partial t} dV + \iint_S W \cdot \nabla c dS = \iint_V \nabla[\kappa \nabla c] ds + \iiint_V s dV$$

An approximation of the local gradient is calculated from a central differencing approach presented in [31]

$$\begin{aligned} \frac{\partial c(X,Y,Z)}{\partial X} &= \frac{c_{i+1,j,k} - c_{i-1,j,k}}{X_{i+1,j,k} - X_{i-1,j,k}} \\ \frac{\partial c(X,Y,Z)}{\partial Y} &= \frac{c_{i,j+1,k} - c_{i,j-1,k}}{Y_{i,j+1,k} - Y_{i,j-1,k}} \\ \frac{\partial c(X,Y,Z)}{\partial Z} &= \frac{c_{i,j,k+1} - c_{i,j,k-1}}{Z_{i,j,k+1} - Z_{i,j,k-1}} \end{aligned} \tag{21}$$

E. Sensor-based grid adaptation and switching

For the state estimation scheme to be useful in the outlined applications, real time implementation is necessary. A reduced dimensional state estimator is utilized, which allows a significant reduction in computational power at the expense of solution accuracy. One technique used to increase accuracy while keeping required computational power low is the application of grid adaptation [36], [37]. Many different techniques are available depending on the problem of interest and usually involve increasing the grid density in areas of interest. In this work, the area of interest is time dependent, suggesting the use of a stretched grid approach.

When working with stretched grids, the spatial operators must be adjusted for each new grid. If the grid is potentially changing throughout the entire simulation, this can become computationally expensive. To avoid this computational cost, a limited number of computational grids is used. Each grid has the same number of computational nodes that can be redistributed to one of twenty seven (3^3) possible grid layouts. Three possible grid configurations are shown in Figure 4. Choosing the available grids before the estimation scheme is started allows the spatial operators as well as the prolongation and restriction matrices to be calculated a priori and stored for faster computations at grid switching intervals.

Simulation of a continuous time process with the discrete grid switching results in a hybrid dynamical system. A state dependent switched system [38] is developed based on the spatial location of the estimated source location Θ_c. As the estimated source location moves throughout the domain, the grid adapts to increase the resolution in that area. The mesh is distributed so that 1/8th of the computational domain has a fine resolution and the rest is coarse. The specific location of the mesh has 3 possible locations in each of the Cartesian directions to account for the equal probability of the area of interest being located anywhere in the domain.

The 27 possible grids produce a family of matrices $\{A_i, i \in \mathcal{I}\}$. The function $\sigma : [0, \infty) \to \mathcal{I}$ is a piecewise

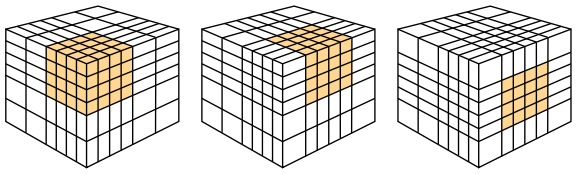

Fig. 4. Three possible grid configurations with the finest resolution volumes highlighted.

switching signal for the spatial operator based on the grid switches. The output matrix $C_i(\Theta_s)$ will also change as the grid changes since it contains the spatial information of the sensor location. The resulting state estimator is then

$$\begin{aligned} \dot{\hat{x}}(t) = &\left(A_i - \gamma C_i^T(\Theta_s(t)) C_i(\Theta_s(t))\right) \hat{x}(t) \\ &+ \gamma C_i^T(\Theta_s(t)) y(t; \Theta_s(t)). \end{aligned} \tag{22}$$

V. Numerical Simulation Results

Two source trajectories are examined to evaluate the performance of the proposed estimation scheme in a 3D domain. In both simulations, a domain size of 4km $\times$4km $\times$1km is used. The flow is evolved in 3D with a constant eddy diffusivity $\kappa_{XX} = \kappa_{YY} = 15\text{m}^2/\text{s}, \kappa_{ZZ} = 5\text{m}^2/\text{s}$, and constant advection, $W_X = 5\text{m/s}, W_Y = 5\text{m/s}, W_Z = 0.5\text{m/s}$. Material is released from the source at a constant rate of 1kg/s. The sensor's velocity is limited to $10\text{m/s} \leq v_s \leq 30\text{m/s}$. While patrolling, the sensor is kept at a constant 15m/s.

A. Stationary Source

A single source is placed in the center of the domain and is releasing material at a constant rate. The sensor begins patrolling and after approximately 60s detects the contaminant and begins the estimation process. The guidance scheme quickly drives the sensor to the middle of the plume where the concentration is highest. The agent then continues to move upwind, heading towards the location of maximum state error.

Figure 5 shows a representative concentration slice at 440s. The entire sensor and source trajectory is also overlaid. Since the source is stationary, it is just a single point.

Due to the fact that the source is continuously releasing material, a local state error will remain in that location. This becomes an area of interest for the guidance scheme, causing the sensor to continue flying around in this area. Figure (6) shows the distance between the location of the maximum

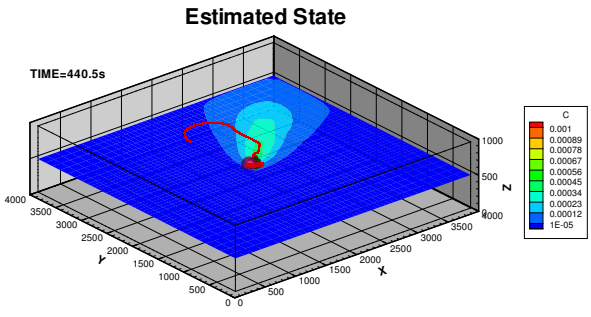

Fig. 5. Estimated source profile slice at $440s$ and $Z = 500m$for a stationary source with source and sensor trajectory overlay.

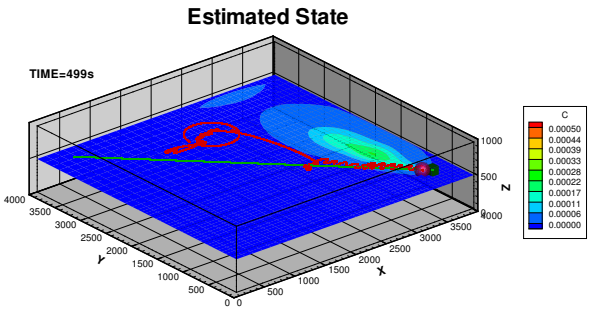

Fig. 7. Estimated source profile slice at 499s and $Z = 550$m for a diagonal source trajectory with source and sensor trajectory overlay.

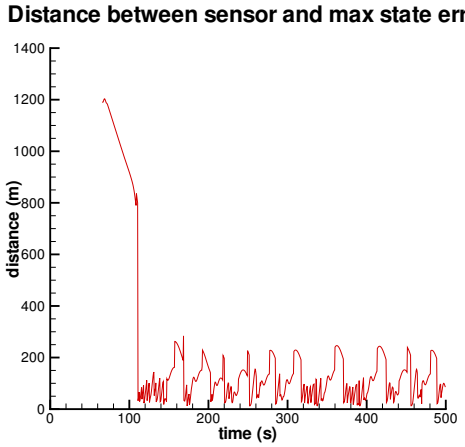

Fig. 6. Distance between sensor and source as a function of time.

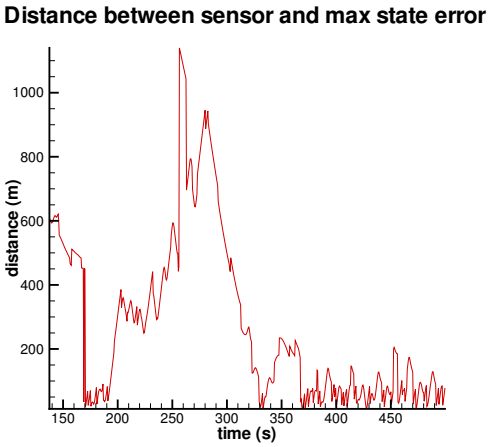

Fig. 8. Distance between sensor and source over time for a diagonal source.

state error and the sensor over time. A distance is not given for times before the estimation scheme is started.

B. Diagonal Source Trajectory

A simple moving source is simulated in which the source passes through the diagonal of the domain at about $10\text{m}/\text{s}$. Similar to the stationary case, the sensor patrolled a given area of the domain until the contaminant was detected, then began estimating the state of the domain. In this case, the results are a bit more interesting. The sensor travels into the plume, passing completely through it, causing a local state error to be eliminated. The sensor then reverses direction, following another state error maximum, until it is again directly in the plume. This time, the sensor travels upwind of the plume until it comes very close to the source. It then meanders down wind of the source for the remaining 150s.

Figure 7 shows a representative concentration slice at 499s with a source and sensor trajectory overlay. The trajectories for the sensor and source are very close near the end of the simulation, indicating that the sensor is following the source.

Due to the fact that this source is continuously releasing material, a local state error will remain near the source location. The guidance scheme will drive the sensor into that region. Figure 6 shows the distance between the location of the maximum state error and the sensor over time. A distance is not given for times before the estimation scheme is started.

VI. Conclusions and Future Work

This paper demonstrates the ability of the model-based estimation scheme for source detection and state estimation. The guidance scheme is shown to drive the sensor in the direction of a higher state error. As the local maxima state errors are reduced, the guidance scheme steers the sensor in the direction of another maximum.

For the case of a continuous source, the guidance scheme not only provide an estimate of the state of the domain, but also an estimate of the location of the source. This information can be very valuable since it can be used to both minimize the impact of the contaminant that has already been released as well as neutralizing the source to prevent more material from being released.

One of the main goals of this work is to provide the state estimate in real time. The simulations presented in this work are based on a mesh of $42 \times 42 \times 18$ cells. This allows the estimation scheme to compute 5x faster than real time on a 2.33Ghz CPU running Linux with Intel's Fortran complier.

Since computational time is below real time, there is room for expansion in increasing the domain size or adding more features to the code.

The current sensor model is an idealized and simplified approach. The sensor assumes noiseless measurements, which would not be available in application. The sensor also assumes state and gradient data is instantaneously available at the sensor location. Atmospheric sensors have a transient response that is affected by their motion, which will be accounted for in future work.

This work provides the state estimation of a contaminant in a three dimensional domain with a single sensor. The use of multiple sensors simultaneously can significantly enhance the state estimation ability of the scheme with a negligible increase in computational requirements.

Many other source behaviors are available for investigation. Two continuous sources have been investigated, however pulsed and instantaneous sources are also provided and can provide significant insight into the capabilities of the estimation scheme.

REFERENCES

[1] M. A. Demetriou, "Centralized and decentralized policies for the containment of moving source in 2D diffusion processes using sensor/actuator network," in *Proc. of the 2009 American Control Conf.*, St. Louis, MO, June 10-12 2009.

[2] M. A. Demetriou and N. A. Gatsonis, "Scheduling of static sensor networks and management of mobile sensor networks for the detection and containment of moving sources in spatially distributed processes," in *Proc. of the 17th Mediterranean Conference on Control and Automation*, Thessaloniki, Greece, June 24-26 2009.

[3] M. A. Demetriou, "Power management of sensor networks for detection of a moving source in 2-D spatial domains," in *Proc. of the 2006 American Control Conference*, Minneapolis, Minnesota, USA, June 14-16 2006.

[4] M. E. Alpay and M. H. Shor, "Model-based solution techniques for the source localization problem," *IEEE Transactions on Control Systems Technology*, vol. 8, no. 6, November 2000.

[5] P. Tzanos and M. Žefran, "Locating a circular biochemical source: Modeling and control," in *Proc. of the 2007 IEEE Int'l Conference on Robotics and Automation*, Roma, Italy, April 10-14 2007.

[6] A. Lilienthal, H. Ulmer, H. Frohlich, A. S. A. amd F. Werner, and A. Zell, "Gas source declaration with a mobile robot," in *Proceedings of the 2004 IEEE International Conference on Robotics & Automation*, New Orleans, LA, April, 2004.

[7] M. A. Demetriou, "Guidance of mobile actuator-plus-sensor networks for improved control and estimation of distributed parameter systems," *IEEE Tr. on Automatic Control*, vol. 55(7), pp. 1570–1584, 2010.

[8] ——, "Detection and containment policy of moving source in 2-D diffusion processes using sensor/actuator network," in *Proc. of the 2007 European Control Conference (ECC 07)*, Kos, Greece, July 2-5 2007.

[9] ——, "Modle-based detection of a moving gaseous source in a 2-D spatial domain using a sensor-based grid adaptation approach," in *Proc. of the 2011 American Control Conference (ACC 11)*, San Francisco, CA, June 29 - July 1 2011.

[10] A. Matveev, H. Teimoori, and A. Savkin, "Navigation of a unicycle-like mobile robot for environmental extremum seeking," *Automatica*, vol. 47, pp. 85–91, 2010.

[11] N. Ghods and M. Krstic, "Source seeking with very slow or drifting sensors," *Journal of Dynamic Systems, Measurement, and Control*, vol. 133, p. 044504, 2011.

[12] J. Cochran and M. Krstic, "Nonholonomic source seeking with tuning of angular velocity," *Automatic Control, IEEE Transactions on*, vol. 54, no. 4, pp. 717–731, 2009.

[13] J. H. Seinfeld and S. N. Pandis, *Atmospheric Chemistry and Physics: From Air Pollution to Climate Change*. New York: Wiley-Interscience, 2006.

[14] S. P. Arya, *Air Pollution Meteorology and Dispersion*. New York: Oxford University Press, 1999.

[15] R. A. Dobbins, *Atmospheric Motion and Air Pollution*. New York: Wiley, 1979.

[16] K. Brzozowski and W. Kotlarz, "Modelling of air pollution on a military airfield," *Atmospheric Environment*, vol. 39(33), pp. 6130–6139, 2005.

[17] N. Koutsourakis, J. Bartzis, A. Venetsanos, and S. Farailidis, "Computation of pollutant dispersion during an airplane take-off," *Environmental Modelling & Software*, vol. 21(4), pp. 486 – 493, 2006.

[18] E. Cespedes and C. Kolb, "Spectroscopic environmental trace species sensors," *Optics & Photonics ews*, vol. 9(8), pp. 38–43, August 1998.

[19] M. Ghanem, Y. Guo, J. Hassard, M. Osmond, and M. Richards, "Sensor grids for air pollution monitoring," in *In Proc. 3rd UK e-Science All Hands Meeting*, 2004.

[20] U. Schumann, H. Schlager, F. Arnold, R. Baumann, P. Haschberger, and O. Klemm, "Dilution of aircraft exhaust plumes at cruise altitudes," *Atmospheric Environment*, vol. 32, no. 18, pp. 3097 – 3103, 1998.

[21] U. Schumann, H. Schlager, F. Arnold, J. Ovarlez, H. Kelder, O. Hov, G. Hayman, I.S.A.Isaksen, J. Staehelin, and P. Whitefield, "Pollution from aircraft emissions in the north atlantic flight corridor: Overview on the polinat projects," *Journal of Geophysical Research*, vol. 105(D3), pp. 3605–3631, February 2000.

[22] U. Schumann, P. Konopka, R. Baumann, R. Busen, T. Gerz, H. Schlager, P.Schulte, and H. Volkert, "Estimate of diffusion parameters of aircraft exhaust plumes near the tropopause from nitric oxide and turbulence measurements," *Journal of Geophysical Research*, vol. 100(D7), pp. 14,147–14,162, July 1995.

[23] W. Ren and R. W. Beard, "Trajectory tracking for unmanned air vehicles with velocity and heading rate constraints," *IEEE Tr. on Contr. Sys. Tech.*, vol. 12(5), pp. 706–716, Sept. 2004.

[24] A. Albagul and Wahyudi, "Dynamic modelling and adaptive traction control for mobile robots," *International Journal of Advanced Robotic Systems*, vol. 1(3), pp. 149–154, 2004.

[25] A. Gholipour and M. Yazdanpanah, "Dynamic tracking control of nonholonomic mobile robot with model reference adaptation for uncertain parameters," in *Proc. of the 2003 European Control Conference*, Cambridge, UK, September 2003.

[26] R. Fierro and F. Lewis, "Control of a nonholonomic mobile robot: Backstepping kinematics into dynamics," *Journal of Robotic Systems*, vol. 14(3), pp. 149–164, 1997.

[27] W. Ren and R. W. Beard, "Clf-based tracking control for uav kinematic models with saturation constraints," in *Proc. of the 42nd IEEE Conference on Decision and Control*, Maui, HI, December 2003.

[28] G. P. Roussos, D. V. Dimarogonas, and K. J. Kyriakopoulos, "3d navigation and collision avoidance for a non-holonomic vehicle," in *Proc. of the 2008 American Control Conf.*, Seattle, WA, June 2008.

[29] L. Schmidt, *Introduction to Aircraft Flight Dynamics*. Virginia: American Institute of Aeronautics and Astronautics, Inc, 1998.

[30] Z. Ya, P. Bhattacharya, H. Mohamadian, H. Majlesein, and Y. Ye, "Equational dynamic modeling and adaptive control of uav," in *Proc. of the 2006 IEEE/SMC International Conf. on System of Systems Engineering*, Los Angels, CA, April 2006.

[31] C. Hirsch, *Numerical Computation of Internal & External Flows*. Oxford, GB: Butterworth-Heinemann, 2007.

[32] H. K. Versteeg and W. Malalasekera, *An Introduction to Computational Fluid Dynamics: The Finite Volume Method*. New York: Wiley-Interscience, 1995.

[33] S. Patankar, *Numerical Heat Transfer and Fluid Flow*. Washington: Hemisphere Publishing Corporation, 1980.

[34] N. A. Gatsonis, M. Demagistris, and R. Erlandson, "Three-dimensional magnetohydrodynamic modeling of plasma jets in north star space experiment," *Journal of Spacecraft and Rockets*, vol. 41, no. 4, pp. 509–520, July Aug 2004.

[35] J. Kaipio and E. Somersalo, *Statistical and Computational Inverse Problems*. New York: Springer, 2004.

[36] W. Briggs, *A Multigrid Tutorial*. Philadelphia: Society for Industrial and Applied Mathematics, 2000.

[37] G. Carey and A. Pardhanani, "Multigrid solution and grid redistribution for convection-diffusion," *International Journal for Numerical Methods in Engineering*, vol. 27, pp. 655–664, September 1989.

[38] D. Liberzon, *Switching in Systems and Control*. Boston: Birkhäuser, 2003.